Understanding the Nature and Strength of Noncovalent Face-to-Face Arene–Fullerene Interactions

Michio Yamada,*[,a] Yukiyo Kurihara,[†a] Masaaki Koizumi,[†a] Kasumi Tsuji,[a] Yutaka Maeda,[a] and Mitsuaki Suzuki[b]

[a]Department of Chemistry, Tokyo Gakugei University, Koganei, Tokyo 184-8501, Japan

[b]Department of Chemistry, Josai University, Sakado, Saitama 350-0295, Japan

[†]These authors contributed equally to the work.

Table of Contents

We use a series of well-defined molecular torsion balance systems to understand the nature and strength of noncovalent face-to-face arene–fullerene interactions.

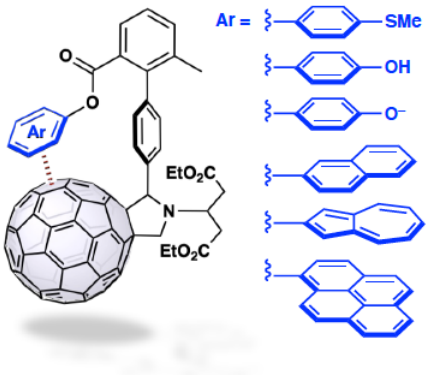

Abstract

Face-to-face noncovalent arene–fullerene interactions are important in several research fields such as synthetic, materials, and medicinal chemistry; however, their nature and strength are still poorly understood. In this study, we prepare a fullerene-based torsion balance containing thioanisole, phenol, naphthalene, azulene, and pyrene moieties as a unimolecular model system. Moreover, we compare the folding free energies between the folded and the unfolded conformers of a series of the molecular

torsion balances to quantify noncovalent interactions between arenes and the fullerene surface. This work demonstrates that the contributions of polarizabilities, anionic charges, electronic dipole moments, and the number of arene rings to the interactions can be experimentally measured by analyzing the folding equilibrium of the molecular torsion balances.

Introduction

Understanding noncovalent interactions, which are ubiquitous in chemical and biological systems, is very important for designing molecular catalysts, controlling macroscopic properties such as morphology and carrier mobility for device applications, and designing inhibitors in medicinal chemistry.[1] Experimental and theoretical studies have been conducted to understand the nature and strength of aromatic interactions between aromatic rings containing planar π-electron systems.[2–4] Curved nanocarbons such as fullerenes and carbon nanotubes containing curved π-electron systems[5] have diverse applications ranging from organic photovoltaics,[6] near-infrared photoluminescent probes and sensors,[7] to HIV protease inhibitors,[8] drug delivery systems,[9] and MRI contrast agents.[10] Therefore, noncovalent interactions at such curved nanocarbons have also attracted growing research interest. Matile et al. have recently proposed the concept of fullerene catalysis, assuming that anion–π interactions act on the fullerene surface between the anionic reaction intermediate and the fullerene-based catalyst.[11] However, direct experimental evidence to determine the strength of such interactions is still lacking. Therefore, quantitative analysis and evaluation of such weak interactions appearing on the curved π-electron systems can contribute to various research fields. To quantify the noncovalent interactions at the fullerene surface, we have recently proposed a unimolecular model system that exhibits two types of conformational isomerism.[12] This system is synthesized by applying the molecular design of a torsion balance.[4b,4e] The torsion balance design consists of pyrrolidinofullerene that is connected to a biaryl structure containing a unit of interest through an ester linkage to verify the interaction between the fullerene surface and the unit, as shown in Figure 1. In the unfolded conformation, the unit of interest moves away from the fullerene surface, whereas in the

folded conformation, the target unit moves closer to the fullerene surface, resulting in noncovalent face-to-face interactions between them. The two conformers are in slow exchange on the ^{1}H NMR timescale; therefore, the signal integration can be used in achieving high precision in the measurements of the folded–unfolded ratios at various temperatures.[13] The interaction between the unit and the fullerene surface can be evaluated using the folding free energies ΔG_{fold} determined from NMR measurements. We observed a linear correlation between ΔG_{fold} and the Hammett constant of the substituent on the benzene unit of interest with respect to the interaction between the benzene ring and the fullerene surface, indicating that electrostatic interactions contribute to the noncovalent face-to-face interactions. Encouraged by these results, we prepared a series of molecular torsion balances containing different arene groups to understand the noncovalent face-to-face interactions between arenes and a fullerene surface. Moreover, we performed conformational analyses to understand the contributions of polarizabilities, anionic charges, electronic dipole moments, and the number of arene rings to these interactions in a quantitative manner. In particular, thioanisole—a sulfur-containing arene, phenol—an acidic proton-containing arene, naphthalene and azulene—simple structural isomers, and pyrene—a typical polyarene containing a large π-electron system—were selected as a unit of interest. Moreover, these arenes (and polyarenes) were introduced to the molecular torsion balance.

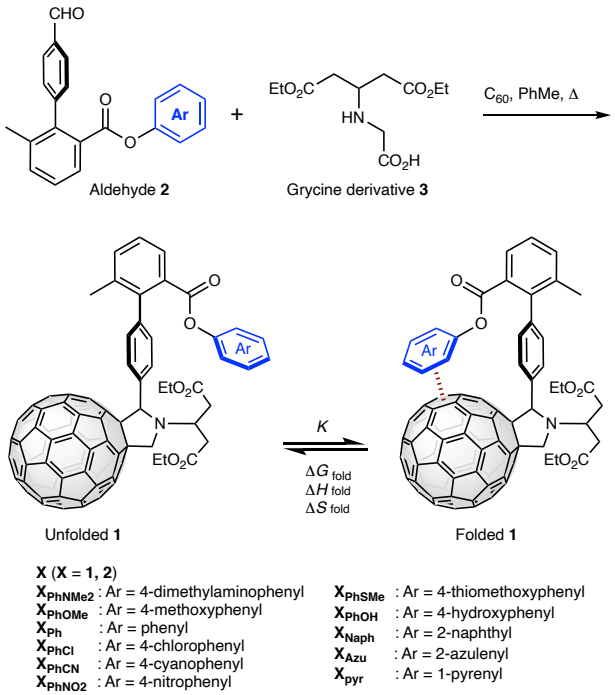

Figure 1. Synthesis route of the molecular torsion balance **1**. The arene ring colored in blue (Ar) represents the unit of interest.

Results and Discussion

Synthesis and Characterization of the Newly Designed Molecular Torsion Balance

The molecular torsion balances bearing 4-thiomethoxyphenyl, 4-hydroxyphenyl, naphthyl, azulenyl, and pyrenyl groups, designated as $\mathbf{1}_{\mathbf{PhSMe}}$, $\mathbf{1}_{\mathbf{PhOH}}$, $\mathbf{1}_{\mathbf{Naph}}$, $\mathbf{1}_{\mathbf{Azu}}$, and $\mathbf{1}_{\mathbf{Pyr}}$, respectively, were newly designed and synthesized using well-established Prato reactions.[14] In short, heating the toluene solution containing C_{60}, aldehyde precursor **2**, and glycine derivative **3** provided the molecular torsion balance **1** in reasonable yields. The molecular torsion balance **1** was isolated by silica gel column chromatography and subsequent gel permeation chromatography. It is noteworthy that $\mathbf{2}_{\mathbf{Azu}}$ was successfully crystallized, and its structure was elucidated using single-crystal X-ray structure analysis, as shown in Figure 2. The dihedral angle around the biaryl group was nearly orthogonal (92.60º), which is important for expressing of two types of conformational isomerism in the torsion balance. The carbon–carbon distance at the periphery of the azulenyl group was 1.39–1.41 Å, confirming that no bond alternation occurred at the azulene π-electron system.

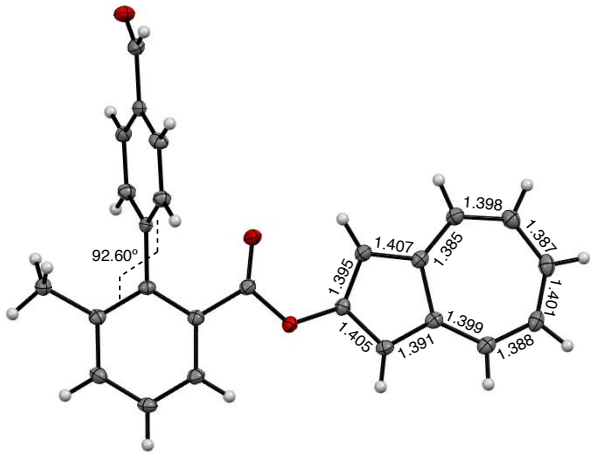

Figure 2. ORTEP diagram of $\mathbf{2}_{\mathbf{Azu}}$ with thermal ellipsoids shown at the 50% probability level. Solvent molecules are omitted for clarity.

The obtained molecular torsion balances were identified by different spectroscopic techniques, including matrix-assisted laser desorption ionization time-of-flight (MALDI-TOF) mass spectrometry, absorption spectroscopy, and NMR. Among the synthesized molecular torsion balances, only $\mathbf{1}_{\mathbf{PhSMe}}$ was found to be unstable in air due to the coexistence of the 4-thiomethoxyphenyl group and a C_{60} core. The HPLC analysis of $\mathbf{1}_{\mathbf{PhSMe}}$ after air exposure exhibited new broad peaks in the very slow retention time region, indicating the formation of highly polar degraded compounds. MALDI-TOF mass spectrometric analysis suggested that the newly formed species are the oxidized species of $\mathbf{1}_{\mathbf{PhSMe}}$ (see Figure S6 in the Supporting Information). In a related work, we reported that photoirradiation of a mixture containing C_{60} and diethyl sulfide in the presence of O_2 yields C_{60} epoxides, diethyl sulfoxide, and diethyl sulfone. Moreover, we found that the persulfoxide intermediate generated by the reaction between diethyl sulfide and in-situ-generated singlet oxygen via energy transfer from $^3C_{60}$* to O_2 participate in the oxidation.[15] Therefore, it is reasonable to consider that exposure of light to $\mathbf{1}_{\mathbf{PhSMe}}$ in air yielded the corresponding sulfoxide and sulfone derivatives of $\mathbf{1}_{\mathbf{PhSMe}}$ (see Figures S4 in the Supporting Information) via a similar reaction mechanism. Because the oxidation proceeded further to provide additionally oxidized species, the sulfide and sulfone derivatives were not isolated nor further analyzed. Therefore, after preparation, the NMR sample of $\mathbf{1}_{\mathbf{PhSMe}}$ was degassed and sealed

immediately, and then conducted for the NMR measurements.

In this study, free energy is the key observable because of its importance in understanding noncovalent interactions in a solution.[1b] The free energy differences between the conformational isomers in the obtained torsional balance molecules were calculated from the signal integral ratios obtained from variable temperature (VT)-^{1}H NMR measurements. The ^{1}H NMR assignments for folded and unfolded conformations were performed based on the comparison between the observed chemical shifts and chemical shifts reported in previous studies.[12] In fact, the methyl protons introduced into the benzene ring of the biaryl group and methine protons at the pyrrolidine ring are well-separated and easily distinguishable for folded and unfolded conformers. To investigate the solvent effects, the VT-^{1}H NMR measurements were conducted in two different solvent environments, that is, $CDCl_3$ and C_6D_6. The thermodynamic parameters obtained in this study are listed in Table 1 in addition to selected data reported in our previous study.[12] Both the folding enthalpy and entropy ΔH_{fold} and ΔS_{fold}, respectively, were determined by fitting linear equations to the experimental data points, although the calculated uncertainty was relatively larger than that of ΔG_{fold} because of the error propagation. As for $\mathbf{1}_{\mathbf{PhOH}}$, VT-^{1}H measurements were conducted before and after adding diisopropylethylamine (DIEA). Moreover, effects of the deprotonation process on the conformational equilibrium were investigated. It is anticipated that at the conformation equilibrium, anion–fullerene interactions contribute to the folding process. Similar experiments were also conducted for $\mathbf{1}_{\mathbf{PhOMe}}$ and $\mathbf{1}_{\mathbf{PhCN}}$ as control experiments.

Table 1. Thermodynamic parameters ΔG_{fold}, ΔH_{fold} and $T\Delta S_{fold}$ of **1** in $CDCl_3$ and C_6D_6.

Compound	ΔG_{fold}[a] / kJ mol^{-1}		ΔH_{fold}[b] / kJ mol^{-1}		$T\Delta S_{fold}$[b] / kJ mol^{-1}	
	$CDCl_3$	C_6D_6	$CDCl_3$	C_6D_6	$CDCl_3$	C_6D_6
$\mathbf{1}_{\mathbf{PhSMe}}$	0.02 ± 0.12	−0.21 ± 0.12	0.26 ± 0.66	5.35 ± 4.87	0.24 ± 0.76	5.56 ± 5.05
$\mathbf{1}_{\mathbf{PhOMe}}$[c]	0.18 ± 0.12	−0.07 ± 0.12	1.09 ± 0.47	3.47 ± 4.87	0.91 ± 0.53	3.54 ± 5.05

$\mathbf{1}_{\mathbf{PhOMe}}$ + DIEA[d]	0.06 ± 0.12	−0.09 ± 0.12	1.40 ± 0.84	3.61 ± 3.14	1.33 ± 0.99	3.69 ± 3.22
$\mathbf{1}_{\mathbf{PhOH}}$	0.57 ± 0.12	1.78 ± 0.12	4.99 ± 0.71	0.01 ± 1.73	4.42 ± 0.84	−1.76 ± 1.75
$\mathbf{1}_{\mathbf{PhOH}}$ + DIEA[d]	0.36 ± 0.12	n/a[e]	5.04 ± 0.66	n/a[e]	4.69 ± 0.76	n/a[e]
$\mathbf{1}_{\mathbf{PhCN}}$[c]	1.14 ± 0.12	1.68 ± 0.12	0.27 ± 0.84	1.80 ± 4.87	−0.87 ± 0.99	0.12 ± 5.05
$\mathbf{1}_{\mathbf{PhCN}}$ + DIEA[d]	0.96 ± 0.12	1.56 ± 0.12	1.77 ± 0.90	2.54 ± 3.14	0.80 ± 1.02	0.98 ± 3.22
$\mathbf{1}_{\mathbf{Ph}}$[c]	0.78 ± 0.12	0.71 ± 0.12	2.09 ± 0.50	1.55 ± 4.87	1.31 ± 0.56	0.83 ± 5.05
$\mathbf{1}_{\mathbf{Naph}}$	−0.71 ± 0.12	−0.34 ± 0.12	0.46 ± 0.84	−3.45 ± 3.14	1.16 ± 0.99	−3.11 ± 3.22
$\mathbf{1}_{\mathbf{Azu}}$	−0.98 ± 0.12	−0.67 ± 0.12	−0.37 ± 0.84	−7.90 ± 4.87	0.61 ± 0.99	−7.24 ± 5.04
$\mathbf{1}_{\mathbf{Pyr}}$	−3.00 ± 0.12	−3.37 ± 0.12	−1.79 ± 0.54	−6.38 ± 4.87	1.21 ± 0.61	−3.01 ± 5.04

[a] The values in the data are averaged over multiple (≥3) measurements at 298 K. For an error analysis see refs. [12–13] and the Electronic Supplementary Information. [b] The values in the data are averaged over multiple (≥3) measurements at 298 K. Uncertainty was estimated using error propagation equations. For details, see the Electronic Supplementary Information. [c] Ref. [12]. [d] DIEA (20 μL) was added to the NMR sample containing **1** in 800 μL of $CDCl_3$. [e] Data not available because of complex signal splitting owing to insufficient deprotonation resulting from the addition of DIEA.

The optimized structures of the folded and unfolded conformers of $\mathbf{1}_{\mathbf{PhSMe}}$, $\mathbf{1}_{\mathbf{PhOH}}$, $\mathbf{1}_{\mathbf{Naph}}$, $\mathbf{1}_{\mathbf{Azu}}$, and $\mathbf{1}_{\mathbf{Pyr}}$ were obtained from density functional theory (DFT) calculations at the M06-2X[16] level of theory using the 6-31G(d)[17] basis sets. The effects of chloroform as the solvent were introduced based on self-consistent reaction field theory calculations performed using the IEFPCM method.[18] As shown in Figure 3, the DFT calculations suggest that all of the five torsion balances prefer folded conformers to unfolded ones. Particularly, the calculated energy difference between the folded and the unfolded conformers in $\mathbf{1}_{\mathbf{Py}}$ is prominent and as large as 17 kJ mol^{-1}. In the optimized structures of the folded conformers, the terminal arene rings are arranged parallel to the fullerene surface to hold the face-to-face configuration with the smallest carbon–carbon distance of 3.1–3.2 Å.

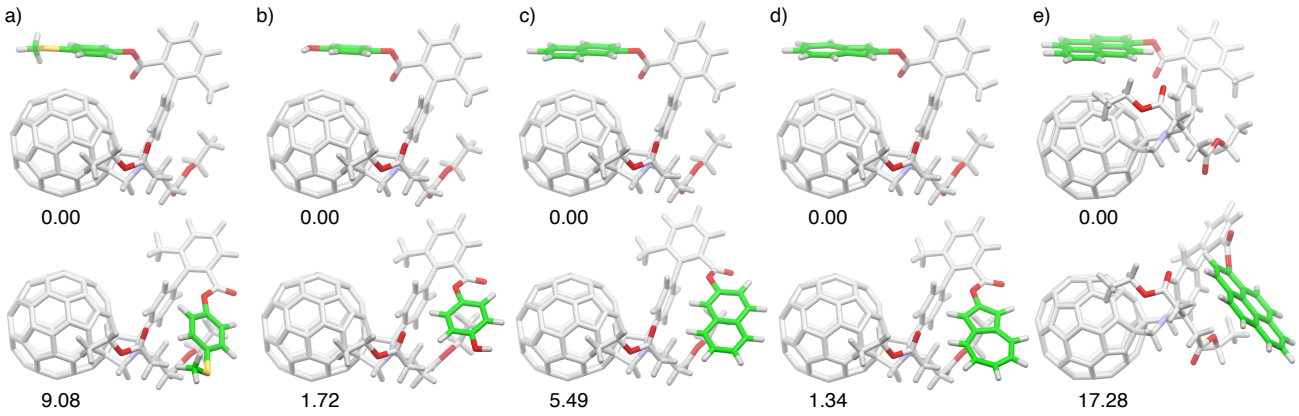

Figure 3. Optimized structures and relative energies (in kJ mol^{-1}) of the folded and unfolded conformers of $\mathbf{1}_{\mathbf{PhSMe}}$, $\mathbf{1}_{\mathbf{PhOH}}$, $\mathbf{1}_{\mathbf{Naph}}$, $\mathbf{1}_{\mathbf{Azu}}$, and $\mathbf{1}_{\mathbf{Pyr}}$ determined using the M06-2X[16]/6-31G(d)[17] level of theory. Effects of chloroform as the solvent were introduced through self-consistent reaction field theory calculations performed using IEFPCM method.[18] The carbon atoms of the terminal arene rings are highlighted in green.

Sulfur-Containing Arene–Fullerene Interactions

The nature of sulfur–arene interactions have been explored extensively in a number of studies because such interactions are abundant in proteins and protein–ligand complexes, where sulfur-containing amino acid side chains (Met and Cys) play a key role.[1a,1e,19] In this context, we first focused on the contribution of sulfur in the noncovalent arene–fullerene interactions by comparing the thermodynamic data of $\mathbf{1}_{\mathbf{PhSMe}}$ with those of $\mathbf{1}_{\mathbf{PhOMe}}$ and $\mathbf{1}_{\mathbf{Ph}}$, as illustrated in Figure 4.

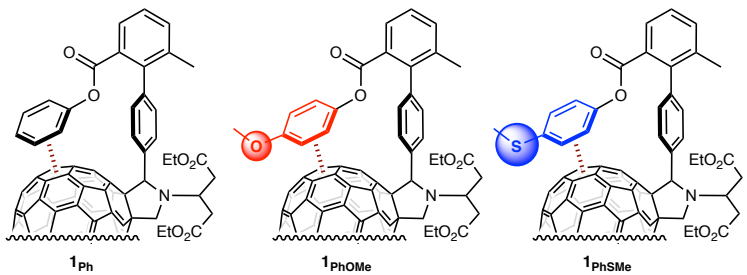

Figure 4. Schematic illustration of the folded conformers of $\mathbf{1}_{\mathbf{Ph}}$, $\mathbf{1}_{\mathbf{PhOMe}}$, and $\mathbf{1}_{\mathbf{PhSMe}}$.

The positive ΔG_{fold} value of $\mathbf{1}_{\mathbf{PhOMe}}$ in $CDCl_3$ indicate that the major contributor in the interaction is

considered to be the Pauli repulsion term. In $CDCl_3$, the difference in the folding free energies of $\mathbf{1}_{\mathbf{PhSMe}}$ and $\mathbf{1}_{\mathbf{PhOMe}}$ was –0.16 kJ mol^{-1}, indicating that the equilibrium shifts toward the folded conformation by replacing the methoxy group with a thiomethoxy group. Moreover, this replacement also reduced the ΔH_{fold} value by 0.83 kJ mol^{-1} (ΔH_{fold} of $\mathbf{1}_{\mathbf{PhOMe}}$ = 1.09 kJ mol^{-1}; ΔH_{fold} of $\mathbf{1}_{\mathbf{PhSMe}}$ = 0.26 kJ mol^{-1}), indicating that the folded conformation of $\mathbf{1}_{\mathbf{PhSMe}}$ is also relatively favored in terms of enthalpy compared to that of $\mathbf{1}_{\mathbf{PhOMe}}$. Figure 5a shows the relationship between the individual ΔG_{fold} values and the Hammett constant for the substituent in the terminal benzene ring. The Hammett constant[20] at the *para* position (σ_{para}) of the thiomethoxy group (σ_{para}= 0) was relatively positive than that of the methoxy group (σ_{para} = –0.27). Nevertheless, $\mathbf{1}_{\mathbf{PhSMe}}$ favored the folded conformation more strongly than $\mathbf{1}_{\mathbf{PhOMe}}$**.** Therefore, the relative preference of the folded conformers for sulfur over oxygen in measuring the conformational equilibrium in $\mathbf{1}_{\mathbf{PhOMe}}$ and $\mathbf{1}_{\mathbf{PhSMe}}$ could be attributed to its higher polarizability values. In addition, significant difference (0.76 kJ mol^{-1}) was observed in the ΔG_{fold} values between $\mathbf{1}_{\mathbf{Ph}}$ and $\mathbf{1}_{\mathbf{PhSMe}}$, even though the σ_{para} values of hydrogen and the thiomethoxy group were zero. In this context, the ΔG_{fold} values between $\mathbf{1}_{\mathbf{Ph}}$ and $\mathbf{1}_{\mathbf{PhSMe}}$ should be identical if the aerne–fullerene interaction was governed solely by the electrostatics of the benzene quadrupoles. Since that is not the case, the relative preference of the folded conformer in $\mathbf{1}_{\mathbf{PhSMe}}$ over those in $\mathbf{1}_{\mathbf{PhOMe}}$ and $\mathbf{1}_{\mathbf{Ph}}$ corresponds to the difference in the dispersion terms. In fact, the polarizability value of thioanisole, which can be recognized as the model for the arene moiety in $\mathbf{1}_{\mathbf{PhSMe}}$, was reported to be 15.9 Å^3,[21] which is larger than those of benzene (10.4 Å^3)[22] and anisole (13.1 Å^3).[22] Figure 5b shows the relationship between ΔG_{fold} and mean polarizability (α) of the corresponding arene molecules (Ar-H). The results indicate that the attractive dispersion interactions play dominant role in the arene–fullerene interactions in $\mathbf{1}_{\mathbf{PhSMe}}$ that is sufficient for overcoming the Pauli repulsive terms between the fullerene and thioanisole moiety. In addition, the ΔG_{fold} value of $\mathbf{1}_{\mathbf{PhSMe}}$ in $CDCl_3$ was within the range of the Hammett constant criterion, suggesting that the location of the attractive interaction can be regarded as the arene–fullerene contact rather than the direct sulfur–fullerene contact. In a related work, Motherwell et al. reported that a oxathilane compound containing a dibenzobicyclo[3,2,2]nonane

scaffold exhibit a preferential S–arene interaction rather than O–arene interaction with the free energy difference of –2.9 kJ mol^{-1} in $CDCl_3$.[23] In C_6D_6, the ΔG_{fold} value of $\mathbf{1}_{\mathbf{PhSMe}}$ was lower than that of $\mathbf{1}_{\mathbf{PhOMe}}$ by 0.14 kJ mol^{-1}. However, the enthalpy and entropy terms exhibited large positive values, suggesting that the competitive solute–solvent interactions and rearrangement of the solvent molecules that are in contact with the solute surface contribute largely to the free energy difference.

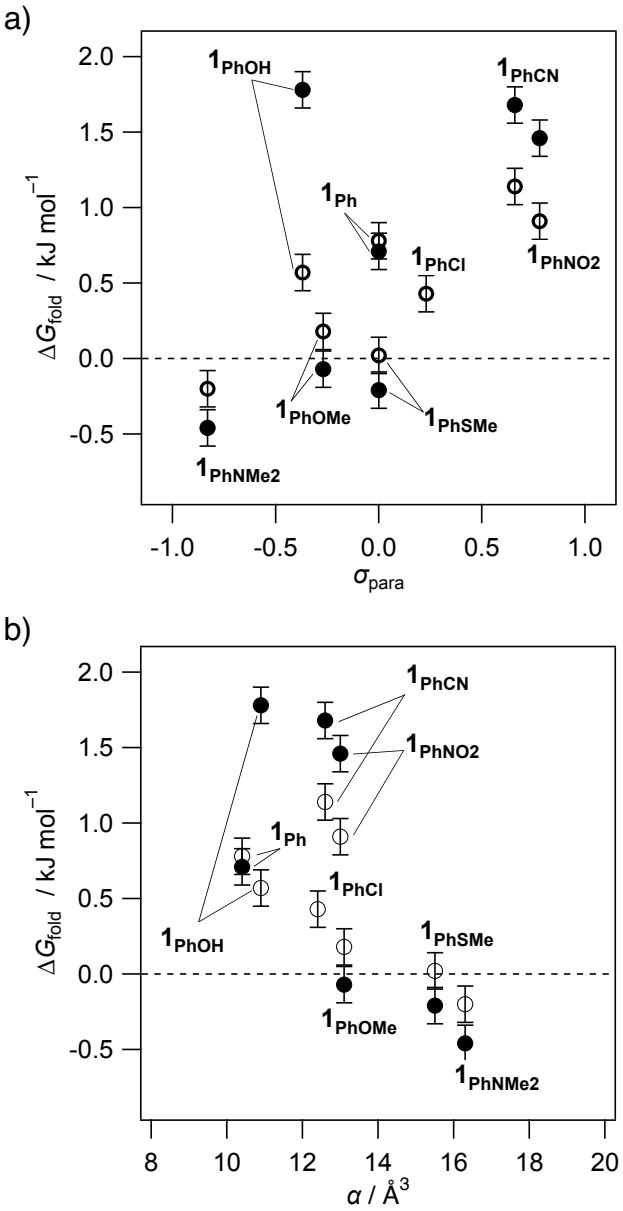

Figure 5. Experimental ΔG_{fold} values in $CDCl_3$ (open circles) and C_6D_6 (solid circles) plotted against the a) Hammett constant σ_{para} values of respective substituents in the terminal benzene ring in **1** and b) mean polarizability (α) values of the corresponding arene molecules (Ar-H). The thermodynamic

data of $\mathbf{1}_{\mathbf{PhNMe2}}$, $\mathbf{1}_{\mathbf{PhOMe}}$, $\mathbf{1}_{\mathbf{Ph}}$, $\mathbf{1}_{\mathbf{PhCl}}$, $\mathbf{1}_{\mathbf{PhCN}}$, and $\mathbf{1}_{\mathbf{PhNO2}}$ were taken from Ref. [12]. The α values were taken from Refs. [21, 22].

Anionic Arene–Fullerene Interactions

Conformational analysis of the molecular torsion balance containing an acidic 4-hydroxyphenyl group, $\mathbf{1}_{\mathbf{PhOH}}$, was performed to evaluate not only the noncovalent interaction between C_{60} and the 4-hydroxyphenyl group but also the interaction between C_{60} and the corresponding phenoxide anion, which can be produced by adding an appropriate base such as DIEA to $\mathbf{1}_{\mathbf{PhOH}}$. The former could be regarded as a model for the interaction between C_{60} and Tyr residues in proteins. In a related work, protein-directed self-assembly of a fullerene crystal was reported by Kim et al., in which the substructure of a C_{60} molecule sandwiched between two Tyr residues was resolved by X-ray crystallography.[24] In addition, the interaction between C_{60} and a phenoxide anion could be regarded as a model for the poorly understood anion–fullerene interactions.[11] As seen in Figure 5, the ΔG_{fold} value of $\mathbf{1}_{\mathbf{PhOH}}$ in $CDCl_3$ is consistent with the correlation line with the Hammett constant obtained in our previous study.[12] However, in C_6D_6, the ΔG_{fold} value of $\mathbf{1}_{\mathbf{PhOH}}$ was significantly far off the linear relationship. The folding enthalpy and entropy terms of $\mathbf{1}_{\mathbf{PhOH}}$ showed relatively large positive values in $CDCl_3$; however, these values decreased significantly in C_6D_6, suggesting that the conformational isomerism was strongly affected by the solute–solvent interactions. This could be because of the acidic character of the hydroxyphenyl group at the terminal benzene ring in $\mathbf{1}_{\mathbf{PhOH}}$. It is likely that in $CDCl_3$, the solvent molecules interact strongly with the surface of the unfolded conformer of $\mathbf{1}_{\mathbf{PhOH}}$ because of its larger molecular surface than the folded conformer. This surface area is reduced when $\mathbf{1}_{\mathbf{PhOH}}$ forms the folded conformer. The large $T\Delta S$ value of $\mathbf{1}_{\mathbf{PhOH}}$ in $CDCl_3$ could be derived from the release of the solvent molecules from the molecular surface. It is also likely that in C_6D_6, the solute–solvent interactions reduce, and solvent molecules prefer to interact with each other, because benzene is a nonpolar and planar molecule.

The deprotonation process of the hydroxy group in $\mathbf{1}_{\mathbf{PhOH}}$ was investigated. The ^1H signals of the

phenolic protons were observed as broad signals and exhibited a characteristic temperature-dependent chemical shift. By adding DIEA, the phenol moiety of $\mathbf{1}_{\mathbf{PhOH}}$ converted to the corresponding phenoxide. In fact, the phenolic proton signal disappeared completely by the addition of DIEA, confirming that the phenolic structure was sufficiently converted to the phenoxide structure under the applied condition in $CDCl_3$, as illustrated in Figure 6a. Therefore, the interaction between phenoxide and fullerene can be observed upon adding DIEA. Similar experiments were conducted for $\mathbf{1}_{\mathbf{PhOMe}}$ and $\mathbf{1}_{\mathbf{PhCN}}$ as control experiments, and the effect of polarity changes of the solvent environment owing to the addition of DIEA on the ΔG_{fold} values was evaluated. This is because the DIEA-induced polarity change of the solvent environment could be inevitable, even if the amount of DIEA added is small. On the other hand, in C_6D_6, insufficient deprotonation was observed upon the addition of DIEA; therefore, the thermodynamic data after the addition of DIEA in C_6D_6 is not presented here. Moreover, adding DIEA decreased the ΔG_{fold} values of $\mathbf{1}_{\mathbf{PhOMe}}$ and $\mathbf{1}_{\mathbf{PhCN}}$ by 0.16 and 0.18 kJ/mol^{-1}, respectively, as summarized in Figure 6b. In the case of $\mathbf{1}_{\mathbf{PhOH}}$, the decrease in the ΔG_{fold} value upon DIEA addition was 0.21 kJ/mol^{-1}. In this context, the difference of approximately 0.03 kJ/mol^{-1} could be attributed to the additional attractive component in the overall interactions. The data corresponding the proposed model system suggest that the direct anion–π interaction between the phenoxide anion and the fullerene surface is weak but measurable.

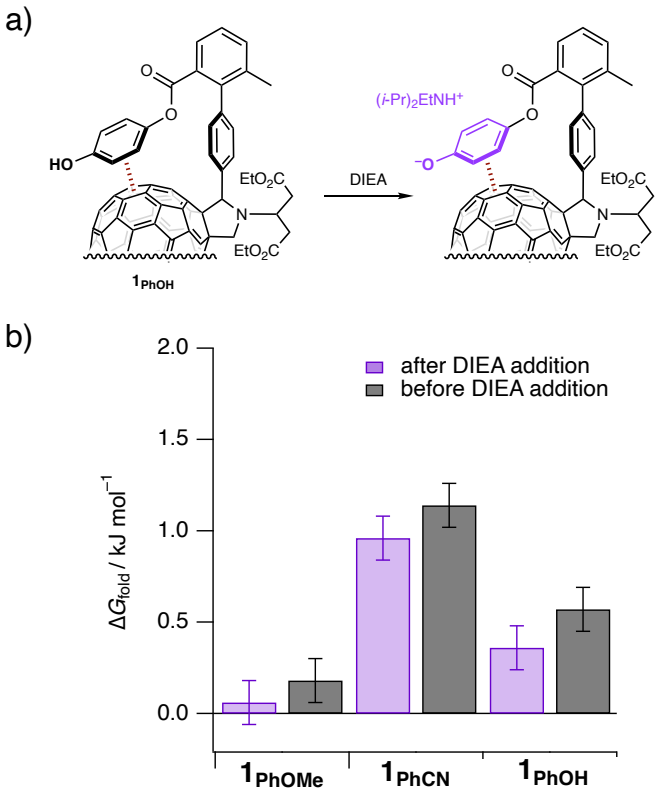

Figure 6. a) Schematic illustration of the partial structures of the folded conformers of $\mathbf{1}_{\mathbf{PhOH}}$ and its deprotonation process. b) Experimental ΔG_{fold} values (in $CDCl_3$) of $\mathbf{1}_{\mathbf{PhOMe}}$, $\mathbf{1}_{\mathbf{PhCN}}$, and $\mathbf{1}_{\mathbf{PhOH}}$ before and after DIEA addition.

Polyarene–Fullerene Interactions

The effect of size in the π–π interactions between arenes and fullerenes can be evaluated by comparing the thermodynamic data of $\mathbf{1}_{\mathbf{Ph}}$, $\mathbf{1}_{\mathbf{Naph}}$, and $\mathbf{1}_{\mathbf{Pyr}}$, because the size of the aromatic rings increases in the following order: benzene, naphthalene, and pyrene. In addition, azulene, which is a structural isomer of naphthalene, is polar and has a dipole moment as large as 1.08 D.[25] Therefore, the contribution of the dipole moment to the interactions can be evaluated by comparing the conformational behaviors of $\mathbf{1}_{\mathbf{Naph}}$ and $\mathbf{1}_{\mathbf{Azu}}$. We first compared the absorption spectra of $\mathbf{2}_{\mathbf{Azu}}$ and $\mathbf{1}_{\mathbf{Azu}}$. The azulene–fullerene electronic interaction was not observed in the absorption spectra. In a related work, Stella et al. reported that the binding constant of the complexation of azulene and C_{60} was too small to be measured in the titration experiments in the concentration range determined by the solubility of C_{60}.[26] On the other

hand, our designed and synthesized torsion balance system allows us to evaluate the azulene–fullerene interaction, which cannot be evaluated by traditional titration experiments.

Figure 7 shows the scattered plots of experimental ΔG_{fold} values and the number of rings in the polyarene unit, and those against the polarizability of the corresponding polyarene molecule (ArH). The data indicated clearly that the ΔG_{fold} values are decreased as the number of rings increased. It is noteworthy that $\mathbf{1_{Pyr}}$ exhibited the most negative ΔG_{fold} values in $CDCl_3$ (–3.00 kJ mol^{-1}) and in C_6D_6 (–3.37 kJ mol^{-1}). The large stabilization of the folded conformers in $\mathbf{1_{Pyr}}$ is consistent with the DFT calculations mentioned above. In addition, the ΔH_{fold} values are also decreased clearly as the number of rings increased, suggesting the existence of a strong noncovalent bonding between the pyrene unit and the fullerene surface. Therefore, it is reasonable to consider that the major contributor of the noncovalent polyarene–fullerene interactions are the dispersion terms. In a related work, Zeinalipour-Yazdi et al. reported that the basis set superposition error (BSSE)-corrected binding energies of face-to-face benzene–polyarene supramolecules at equilibrium separation exhibit a linear relationship with the number of carbon atoms in the supramolecules.[27] Moreover, the static polarizabilities exhibit a similar linear dependence with the number of carbon atoms. The difference in the BSSE-corrected binding energies between benzene–benzene and naphthalene–benzene was calculated to be 6.2 kJ mol^{-1}. In this context, the calculated interactions between planar polyarenes and benzene, which are stronger compared to those between polyarenes and fullerenes measured in this work, could be derived from the effective stacking geometries in the planar π-electron systems. Azulene has lower polarizability (15.5 Å^3) than naphthalene ((17.4 Å^3);[28] therefore, it can be assumed that the naphthalene–fullerene interaction will be stronger than the azulene–fullerene interaction. However, our results show that the ΔG_{fold} values of $\mathbf{1_{Azu}}$ in $CDCl_3$ (–0.98 kJ mol^{-1}) and C_6D_6 (–0.67 kJ mol^{-1}) are more negative than those of $\mathbf{1_{Naph}}$ (–0.71 kJ mol^{-1} in $CDCl_3$ and –0.34 kJ mol^{-1} in C_6D_6). This observation suggests stronger interaction between azulene and fullerene than that between naphthalene and fullerene. Therefore, it is considered that the observed free energy difference between $\mathbf{1_{Naph}}$ and $\mathbf{1_{Azu}}$ was mainly caused by the contribution of the dipole moment of the azulene moiety. Thus, it is

suggested that the polar component of the noncovalent interaction is attractive and as large as ~0.3 kJ mol^{-1} for the system studied here.

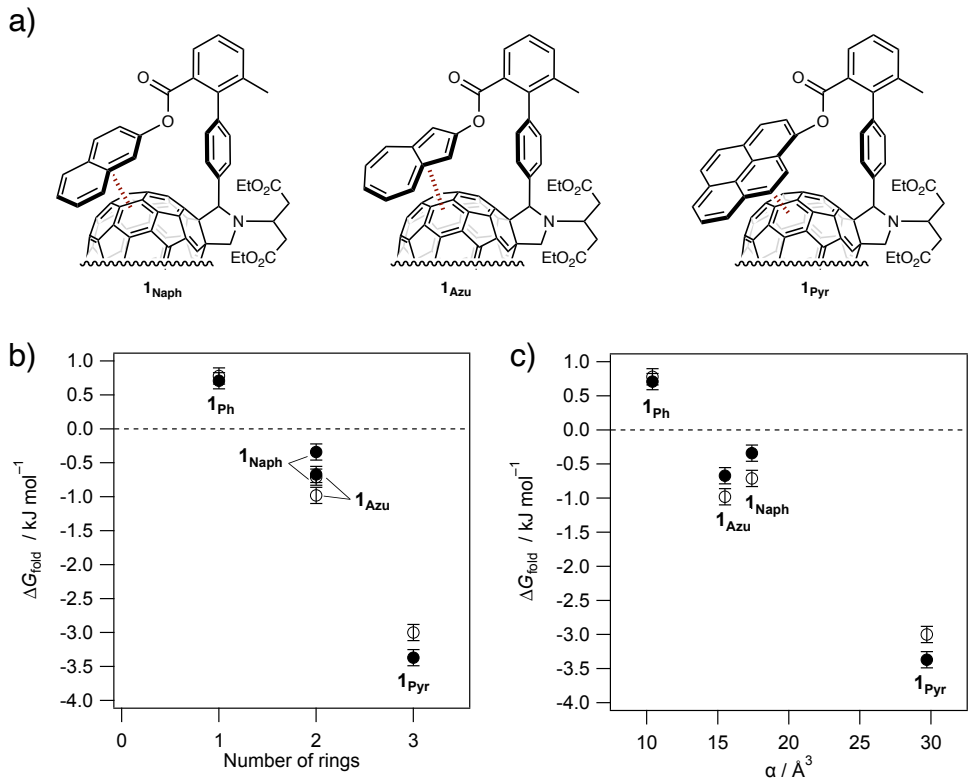

Figure 7. a) Schematic illustration of the partial structures of the folded conformers of $\mathbf{1}_{\mathbf{Naph}}$, $\mathbf{1}_{\mathbf{Azu}}$, and $\mathbf{1}_{\mathbf{Pyr}}$. Experimental ΔG_{fold} values of $\mathbf{1}_{\mathbf{Naph}}$, $\mathbf{1}_{\mathbf{Azu}}$, and $\mathbf{1}_{\mathbf{Pyr}}$ in $CDCl_3$ (open circles) and C_6D_6 (solid circles) plotted against the b) number of rings in the polyarene unit in **1** and c) mean polarizability (α) values of the corresponding polyarene molecules (Ar-H). The thermodynamic data of $\mathbf{1}_{\mathbf{Ph}}$ were taken from Ref. [12]. The α values were taken from Refs. [28].

Conclusion

We synthesized a new series of fullerene-based molecular torsion balances and examined their folding equilibrium to understand the nature and strength of noncovalent face-to-face arene–fullerene interactions. Based on the conformational analysis using VT-^{1}H NMR spectroscopy, we draw the following conclusions. First, the contribution of electrostatic interactions to the arene–fullerene interactions could be evaluated from the linear relationship between the folding free energies and the

Hammett constants of the substituents of the benzene ring. The free energy difference between $\mathbf{1}_{\mathbf{Ph}}$ and $\mathbf{1}_{\mathbf{PhSMe}}$ in $CDCl_3$ was found to be 0.76 kJ mol^{-1}, indicating that dispersion interactions play an important role in the overall interactions. Direct interactions between sulfur and the fullerene surface were not observed clearly in $\mathbf{1}_{\mathbf{PhSMe}}$. Instead, the presented data suggested that the interaction between the thioanisole moiety and the fullerene surface could be explained based on the Hammett constant criterion. Second, measurements of the noncovalent interaction between an anionic arene moiety and the fullerene surface were achieved through deprotonation of $\mathbf{1}_{\mathbf{PhOH}}$ by adding DIEA. The net decrease in the folding free energy by 0.03 kJ/mol^{-1} following the deprotonation could be attributed to the anion–π interaction between the phenoxide anion and the fullerene surface. However, the difference was very small, and any special attractive force related to the anionic charges was not observed in the presented model system. Third, in the noncovalent polyarene–fullerene interactions in $\mathbf{1}_{\mathbf{Ph}}$, $\mathbf{1}_{\mathbf{Naph}}$, $\mathbf{1}_{\mathbf{Azu}}$, and $\mathbf{1}_{\mathbf{Pyr}}$, the folding free energies became more negative values as the number of rings in the polyarenes increased. The difference in the folding free energies was 3.78 kJ/mol^{-1} in $CDCl_3$ and 4.08 kJ/mol^{-1} in C_6D_6. The strong stabilization of the folded conformers in the polyarene–fullerene systems could be due to the large polarizabilities of the polyarenes. Finally, the contributions of the electronic dipole moment to the arene–fullerene interactions were investigated by comparing the thermodynamic data of $\mathbf{1}_{\mathbf{Naph}}$ and $\mathbf{1}_{\mathbf{Azu}}$, and found to be as large as 0.27 kJ/mol^{-1} in $CDCl_3$ and 0.33 kJ mol^{-1} in C_6D_6. We believe that the present quantitative analysis will provide valuable data to guide the design of nanocarbon-based functional materials.

Acknowledgement

This work was supported by the Asahi Glass Foundation and was partly supported by JSPS KAKENHI Grant Number JP20K05472. This article is dedicated to the memory of Prof. François Diederich—a great mentor and a great contributor to the fields of molecular recognition and host–guest chemistry, new allotropes of carbon and novel carbon-rich molecules, and drug activity and design.

Conflict of Interest

The authors declare no conflict of interest.

Keywords:

Hammett analysis, π–π interactions, anion– π interactions, London dispersion force, electrostatic interactions, fullerenes

References

1. a) E. A. Meyer, R. K. Castellano, F. Diederich, *Angew. Chem.* **2003**, *115*, 1244–1287; *Angew. Chem. Int. Ed.* **2003**, *42*, 1210–1250; b) C. A. Hunter, *Angew. Chem.* **2004**, *116*, 5424–5439; *Angew. Chem. Int. Ed.* **2004**, *43*, 5310–5324; c) M. Nishio, *CrystEngComm* **200**4, *6*, 130–158; d) K. Müller, C. Faeh, F. Diederich, *Science* **2007**, *317*, 1881–1886; e) L. M. Salonen, M. Ellermann, F. Diederich, *Angew. Chem.* **2011**, *123*, 4908–4944; *Angew. Chem. Int. Ed.* **2011**, *50*, 4808–4842; f) *Noncovalent Forces. Challenges and Advances in Computational Chemistry and Physics*, *Vol. 19* (Ed.: S. Scheiner), Springer, Cham, **2015**; f) M. Y. Jin, Q. Zhen, D. Xiao, G. Tao, X. Xing, P. Yu, C. Xu, *Nat. Commun.* **2022**, *13*, 3276; doi: 10.1038/s41467-022-31026-8.
2. *Aromatic Interactions: Frontiers in Knowledge and Application* (Eds.: D. W. Johnson, J. Fraser Hof), The Royal Society of Chemistry, Cambridge, **2017.**
3. a) M. O. Sinnokrot, C. D. Sherrill, *J. Phys. Chem. A* **2003**, *107*, 8377–8379; b) M. O. Sinnokrot, C. D. Sherrill, *J. Phys. Chem. A* **2006**, *110*, 10656–10668; c) S. E. Wheeler, K. N. Houk, *J. Am. Chem. Soc.* **2008**, *130*, 10854–10855; d) S. Grimme, *Angew. Chem.* **2008**, *120*, 3478–3483; *Angew. Chem. Int. Ed.* **2008**, *47*, 3430–3434; e) A. L. Ringer, C. D. Sherrill, *J. Am. Chem. Soc.* **2009**, *131*, 4574–4575; f) S. E. Wheeler, A. J. McNeil, P. Müller, T. M. Swager, K. M. Houk, *J. Am. Chem. Soc.* **2010**, *132*, 3304–3311; g) S. E. Wheeler, *J. Am. Chem. Soc.* **2011**, *133*, 10262–10274; h) M. Watt, L. K. E. Hardebeck, C. C. Kirkpatrick, M. Lewis, *J. Am. Chem. Soc.* **2011**, *133*, 3854–3862; i) C. D. Sherrill, *Acc. Chem. Res.* **2013**, *46*, 1020–1028; j) M.-M. Ki, Y.-B. Wang, Y. Zhang, W.

Wang, *J. Phys. Chem. C* **2016**, *120*, 5766–5772.

4. a) C. A. Hunter, J. K. M. Sanders, *J. Am. Chem. Soc.* **1990**, *112*, 5525–5534; b) S. Paliwal, S. Geib, C. S. Wilcox, *J. Am. Chem. Soc.* **1994**, *116*, 4497–4498; c) F. Cozzi, J. S. Siegel, *Pure Appl. Chem.* **1995**, *67*, 683–689; d) R. R. Gardner, L. A. Christianson, S. H. Gellman, *J. Am. Chem. Soc.* **1997**, *119*, 5041–5042; e) E. Kim, S. Paliwal, C. S. Wilcox, *J. Am. Chem. Soc.* **1998**, *120*, 11192–11193; f) C. A. Hunter, K. R. Lawson, J. Perkins, C. J. Urch, *J. Chem. Soc. Perkin Trans.* 2 **2001**, *5*, 651–669; g) S. L. Cockroft, C. A. Hunter, *Chem. Commun.* **2006**, 3806–3808; h) S. L. Cockroft, J. Perkins, C. Zonta, H. Adams, S. E. Spey, C. M. R. Low, J. G. Vinter, K. R. Lawson, C. J. Urch, C. A. Hunter, *Org. Biomol. Chem*. **2007**, *5*, 1062–1080; i) W. R. Carroll, P. Pellechia, K. D. Shimizu, *Org. Let.* **2008**, *10*, 3547–3550; j) S. L. Cockroft, C. A. Hunter, *Chem. Commun.* **2009**, 3961–3963; k) Y. S. Chong, W. R. Carroll, W. G. Burns, M. D. Smith, K. D. Shimizu, *Chem. Eur. J.* **2009**, *15*, 9117–9126; l) J. L. Xia, S. H. Liu, F. Cozzi, M. Mancinelli, A. Mazzanti, *Chem. Eur. J.* **2012**, *18*, 3611–3620; m) H. Gardarsson, W. B. Schweizer, N. Trapp, F. Diederich, *Chem. Eur. J.* **2014**, *20*, 4608–4616; n) J. Hwang, B. E. Dial, P. Li, M. E. Kozik, M. D. Smith, K. D. Shimizu, *Chem. Sci.* **2015**, *6*, 4358–4364; o) S. Yamada, N. Yamamoto, E. Takamori, *J. Org. Chem.* **2016**, *81*, 11819–11830; p) L.-J. Riwar, N. Trapp, B. Kuhn, F. Diederich, *Angew. Chem.* **2017**, *129,* 11405–11410; *Angew. Chem. Int. Ed.* **2017**, *56*, 11252–11257; q); z) A. E. Aliev, W. B. Motherwell, *Chem. Eur. J.* **2019**, *25*, 10516–10530; r) C. Bravin, J. A. Piekos, G. Licini, C. A. Hunter, C. Zonta, *Angew. Chem.* **2021**, *133*, 24064–24070; *Angew. Chem. Int. Ed.* **2021**, *60*, 23871–12877.

5. a) T. Kawase, H. Kurata, *Chem. Rev.* **2006**, *106*, 5250–5273; b) *Chemistry of Nanocarbons* (Eds.: T. Akasaka, F. Wudl, S. Nagase)*,* John Wiley & Sons, Chichester, **2010**.

6. a) G. Yu, J. Gao, J. C. Hummelen, F. Wudl, A. J. Heeger, *Science* **1995**, *270*, 1789–1791; b) S. E. Shaheen, C. J. Brabec, N. S. Sariciftci, *Appl. Phys. Lett.* **2001**, *78*, 841–843; c) G. Li, V. Shrotriya, J. Huang, Y. Yao, T. Moriarty, K. Emery, Y. Yang, *Nat. Mater.* **2005**, *4*, 864–868; d) M. C. Scharber, D. Mühlbacher, M. Koppe, P. Denk, C. Waldauf, A. L. Heeger, C. J. Brabec, *Adv. Mater.* **2006**, *18*,

789–794; e) C. Carati, N. Gasparini, S. Righi, F. Tinti, V. Fattori, A. Savoini, A. Cominetti, R. Po, L. Bonoldi, N. Camaioni, *J. Phys. Chem. C* **2016**, *120*, 6909–6919; f) S. Collavini, J. L. Delgado, *Sustainable Energy Fuels* **2018**, *2*, 2480–2493.

7. a) A. M. Smith, M. C. Mancini, S. Nie, *Nat. Nanotechnol.* **2009**, *4*, 710–711; b) S. Ghosh, S. M. Bachilo, R. A. Simonette, K. M. Beckingham, R. B. Weisman, *Science*, **2010**, *330*, 1656–1659; c) K. Welsher, S. P. Sherlock, H. Dai, *Proc. Natl. Acad. Sci. USA* **2011**, *108*, 8943–8948; d) R. Langenbacher, J. Budhathoki-Uprety, P. V. Jena, D. Roxbury, J. Streit, M. Zheng, D. A. Heller, *Nano Lett.* **2021**, *21*, 6441–6448; e) J. Ackermann, J. T. Metternich, S. Herbertz, S. Kruss, Angew. Chem. **2022**, e202112372; *Angew. Chem. Int. Ed*. **2022**, *61*, e202112372.
8. a) S. H. Friedman, D. L. DeCamp, R. P. Sijbesma, G. Srdanov, F. Wudl, G. L. Kenyon, J. *Am. Chem. Soc.***1993**, *115*, 6506–6509; b) R. Sijbesma, G. Srdanov, F. Wudl, J. A. Castoro, C. Wilkins, S. H. Friedman, D. L. DeCamp, G. L. Kenyon, *J. Am. Chem. Soc.* **1993**, *115*, 6510–6512; c) Z. S. Martinez, E. Castro, C,-S. Seong, M. R. Cerón, L. Echegoyen, M. Llano, *Antimicrob. Agents Chemother.* **2016**, *60*, 5731–5741.
9. a) P. P. Fatouros, F. D. Corwin, Z.-J. Chen, W. C. Broaddus, J. L. Tatum, B. Kettenmann, Z. Ge, H. W. Gibson, J. L. Russ, A. P. Leonard, J. C. Duchamp, H. C. Dorn, *Radiology*, **2006**, *240*, 756–764; b) K. Braun, L. Dunsch, R. Pipkorn, M. Bock, T. Baeuerle, S. Yang, W. Waldeck, M. Wiessler, *Int. J. Med. Sci.* **2010**, *7*, 136–146; c) K. B. Ghiassi, M. M. Olmstead, A. L. Balch, *Dalton Trans.* **2014**, *43*, 7346–7358.
10. a) T. Y. Zakharian, A. Seryshev, B. Sitharaman, B. E. Gilbert, V. Knight, L. J. Wilson, *J. Am. Chem. Soc.* **2005**, *127*, 12508–12509. b) J. M. Ashcroft, D. A. Tsyboulski, K. B. Hartman, T. Y. Zakharian, J. W. Marks, R. B. Weisman, M. G. Rosenblum, L. J. Wilson, *Chem. Commun.* **2006**, 3004–3006.
11. a) J. López-Andarias, A. Frontera, S. Matile, *J. Am. Chem. Soc.* **2017**, *139*, 13296–13299; b) J. López-Andarias, A. Bauzá, N. Sakai, A. Frontera, S. Matile, ; *Angew. Chem.* **2018**, *130*, 11049–11053; *Angew. Chem. Int. Ed.* **2018**, *57*, 10883–10887; c) X. Zhang, L. Liu, J. López-Andarias, C. Wang, N. Sakai, S. Matile, *Helv. Chim. Acta* **2018**, *101*, e1700288.

12. M. Yamada, H. Narita, Y. Maeda, *Angew. Chem.* **2020**, *132*, 16267–16274; *Angew. Chem. Int. Ed.* **2020**, *59*, 16133–16140.

13. M. Bauer, A. Bertario, G. Boccardi, X. Fontaine, R. Rao, D. Verrier, *J. Pharm. Biomed. Anal.* **1998**, *17*, 419–425.

14. a) M. Maggini, G. Scorrano, M. Prato, *J. Am. Chem. Soc.* **1993**, *115*, 9798–9799; b) M. Prato, M. Maggini, *Acc. Chem. Res.* **1998**, *31*, 519–526.

15. Y. Maeda, Y. Niino, T. Kondo, M. Yamada, T. Hasegawa, T. Akasaka, *Chem. Lett.* **2011**, 1431–1432.

16. a) Y. Zhao, D. G. Truhlar, *Acc. Chem. Res.* **2008**, *41*, 157–167; b) Y. Zhao, D. G. Truhlar, *Theor. Chem. Acc.* **2008**, *120*, 215–241.

17. W. J. Hehre, R. Ditchfield, J. A. Pople, *J. Chem. Phys.* **1972**, *56*, 2257–2261.

18. M. Cossi, N. Rega, G. Scalmani, V. Barone, *J. Comput. Chem.* **2003**, *24*, 669–681.

19. a) K. S. C. Reid, P. F. Lindley, J. M. Thornton, *FEBS Lett.* **1985**, *190*, 209–213; b) S. K. Burley, G. A. Petsko, *Adv. Protein Chem.* **1988**, *39*, 125–189; c) D. Pal, P. Chakrabarti, *J. Biomol. Struct. Dyn.* **1998**, *15*, 1059–1072; d) R. J. Zauhar, C. L. Colbert, R. S. Morgan, W. J. Welsh, *Biopolymers* **2000**, *53*, 233–248; e) G. Duan, V. H. Smith, Jr., D. F. Weaver, *Mol. Phys.* **2001**, *99*, 1689–1699; f) D. Pal, P. Charkrabarti, *J. Biomol. Struct. Dyn.* **2001**, *19*, 115–128.

20. C. Hansch, A. Leo, R. W. Taft, *Chem. Rev.* **1991**, *91*, 165–195.

21. M. Oftadeh, S. Naseh, M. Hamadanian, *Comput. Theor. Chem.* **2011**, *966*, 20–25.

22. R. Bosque, J. Sales, *J. Chem. Inf. Comput. Sci*. **2002**, *42*, 1154–116.

23. a) W. B. Motherwell, J. Moise, A. E. Aliev, M. Nic, S. J. Coles, P. N. Horton, M. B. Hursthouse, G. Chessari, C. A. Hunter, J. G. Vinter, *Angew. Chem.* **2007**, *119*, 7969–7972; *Angew. Chem. Int. Ed.* **2007**, *46*, 7823–7826; b) W. B. Motherwell, R. B. Moreno, I. Pavlakos, J. R. T. Arendorf, T. Arif, G. J. Tizzard, S. J. Coles, A. E. Aliev, *Angew. Chem.* **2018**, *130*, 1207–1212; *Angew. Chem. Int. Ed.* **2018**, *57*, 1193–1198.

24. K.-H. Kim, D.-K. Ko, Y.-T. Kim, N. H. Kim, J. Paul, S.-Q. Zhang, C. B. Murray, R. Acharya, W.

F. DeGrado, Y. H. Kim, G. Grigoryan, *Nat. Commun*., **2016**, *7*, 11429; doi: 10.1038/ncomms11429.

25. A. G. Anderson Jr., B. M. Steckler, *J. Am. Chem. Soc.* **1959**, *81*, 4941–4946.

26. L. Stella, A. L. Capodilupo, M. Bietti, *Chem. Commun.*, **2008**, 4744-4746.

27. C. D. Zeinalipour-Yazdi, D. P. Pullman, *J. Phys. Chem. B* **2006**, *110*, 24260–24265.

28. M. Gussoni, M. Rui, G. Zerbi, *J. Mol. Struct.* **1998**, *447*, 163–215.